JOC The Journal of Organic Chemistry

Article

pubs.acs.org/joc

Donor–Acceptor–Donor Thienopyrazines via Pd-Catalyzed C–H Activation as NIR Fluorescent Materials

Louis E. McNamara, Nalaka Liyanage, Adithya Peddapuram, J. Scott Murphy, Jared H. Delcamp,* and Nathan I. Hammer*

Department of Chemistry and Biochemistry, University of Mississippi, University, Mississippi 38677, United States

Supporting Information

ABSTRACT: A series of thienopyrazine-based donor–acceptor–donor (D–A–D) near-infrared (NIR) fluorescent compounds were synthesized through a rapid, palladium-catalyzed C–H activation route. The dyes were studied through computational analysis, electrochemical properties analysis, and characterization of their photophysical properties. Large Stokes shifts of approximately 175 nm were observed, which led to near-infrared emission. Computational evaluation shows that the origin of this large Stokes shift is a significant molecular reorganization particularly about the D–A bond. The series exhibits quantum yields of up to φ = >4%, with emission maxima ranging from 725 to 820 nm. The emission is strong in solution, in thin films, and also in isolation at the single-molecule level. Their stable emission at the single-molecule level makes these compounds good candidates for single-molecule photon sources in the near-infrared.

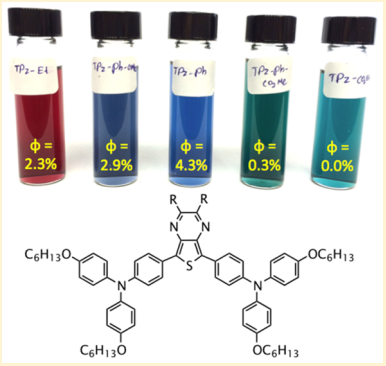

INTRODUCTION

Near-infrared (NIR) emissive organic molecules are an emerging class of materials that have attracted much interest due to their applications in optical and electronic areas.[1−8] Applications of these materials range from use in night-vision technologies, secure communications, fluorescence imaging, transparent photovoltaics, and heat-blocking coating.[8−21] In particular, in vivo fluorescence imaging is a rapidly growing, medical diagnostic technique that makes the development of stable NIR fluorescent tags of great interest.

The development of stable NIR-emitting molecules is complicated by the energy-gap law, which inherently disfavors emission from systems with low-energy band gaps.[22] The most common strategy for the development of organic NIR emitters is to design large π-conjugated systems containing electron-donating (D) and -accepting (A) groups.[1,3,4,23−33] Intramolecular charge transfer (ICT) between the constituent groups results in NIR absorption and emission. However, molecules containing large π-systems with these features tend to aggregate, often resulting in aggregation-induced quenching of emission. This aggregation significantly impairs the process of designing efficient NIR emitters in the condensed state. Despite these intrinsic challenges, narrow band gap organic compounds containing donor–acceptor (D–A) type chromophores are of great interest, since their band gap energy, and other properties, can easily be tuned through varying the donor and acceptor substituents. Here, we report a new series of (D–A–D) thienopyrazines and demonstrate their promise as NIR emitters in solution, while dispersed in a polymer thin film, and at the single-molecule level.

NIR D–A–D dye design relies on the incorporation of substantially electron deficient building blocks to serve as a single acceptor. Thienopyrazines (TPzs) are attractive, unique acceptor building blocks, as four substitutable positions allow for the installation of two donors and allow access to two additional tunable positions.[34−36] The pyrazine ring is electron-deficient and the relatively low resonance stabilization energy of thiophene allows for better ICT between the donor groups and the accepting pyrazine than benzene-based aromatics. Additionally, TPz allows for increased planarity of donor substituents at the thiophene when compared with benzene-based acceptors due to the use of a less sterically encumbered five-membered ring and the use of a ring-contained nitrogen atom at the ortho position relative to the donor group. This increased planarity leads to increased charge transfer band strength to access lower-energy wavelengths and increased absorption strength. We sought to better understand the ground- and excited-state energy level influence of substituents on the pyrazine ring through targeting a series of dyes with the TPz thiophene substituents held constant.

To investigate the effects of the TPz bridge-based dyes on NIR emissive and energetic properties, we have targeted five D–A–D dyes based on the thienopyrazine acceptor with the bis(hexyloxy)triphenylamine (TPA) donor held constant throughout on the thiophene ring while varying the substituents on the pyrazine ring to evaluate the effects on the emissive properties of these materials (Figure 1). The pyrazine ring substituents were varied from alkyl groups, ester groups, and a series of phenyl substituents bearing electron-donating groups (OMe), electron-neutral groups (H), and electron-withdrawing groups (CO_2Me).

Received: August 21, 2015
Published: November 24, 2015

DOI: 10.1021/acs.joc.5b01958
J. Org. Chem. 2016, 81, 32−42

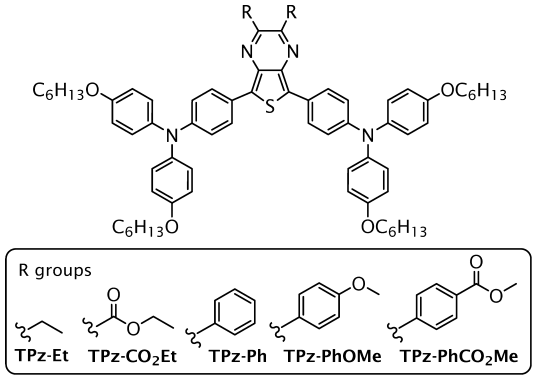

Figure 1. TPz-based target NIR emissive materials TPz−Et, TPz−CO_2Et, TPz−Ph, TPz−PhOMe, and TPz−$PhCO_2$Me created by varying the 2,3-substituents of the TPz ring from electron-donating to electron-withdrawing substituents.

RESULTS AND DISCUSSION

Synthesis. Ideally, D−A−D dyes should be rapidly accessible for simplicity in evaluating structure−function relationships. Direct C−H activation reactions utilizing the C−H bonds of the thiophene ring of the TPz acceptor provide a direct, attractive synthetic route. Therefore, palladium-catalyzed C−H activation routes were evaluated for the synthesis of the TPz dye series. A series of TPz-based D−A−D dyes (Figure 1) was synthesized with variable 2,3-substituents based on a range of conjugated and nonconjugated substituents to identify the electronic and steric effects on performances.[37−39] The syntheses of the TPz-based D−A−D dyes were carried out in four linear steps according to Scheme 1.

The synthetic route to the TPz D−A−D dyes began with the nitration of the commercially available 2,5-dibromothiophene **1** to give 2,5-dibromo-3,4-dinitrothiophene **2** in preparative yield (52%).[40] The reduction of **2** with Sn powder in acidic medium leads to the formation of 3,4-diaminothiophene dihydrochloride **3** in high yield (75%).[40] **3** underwent condensation reactions with the appropriate diketone (3,4-hexanedione, diethyl 2,3-dioxosuccinate, benzil, or 4,4′-oxalyldibenzoate) in a basic environment to give the desired TPz building blocks **4a**−**4c** and **4e** (85%−34% yield).[36,41,42] Condensation with electron-rich 4,4′-dimethoxybenzil required alternate conditions involving a $SnCl_2/SiO_2$ solid support Lewis acid catalyst to give appreciable amounts of **4d** (44%).[43] Finally, the TPz D−A−D dyes (TPz−Et, TPz−CO_2Et, TPz−Ph, TPz−PhOMe, TPz−$PhCO_2$Me) were obtained by Pd-catalyzed direct C−H arylation reaction of **4a**−**4e** in yields ranging from 68%−35% with the use of X-Phos[38] or P*t*Bu_3[39] as ligand. The palladium-catalyzed C−H activation conditions were optimized with TPz−Et. The use of P(*t*Bu)$_3$ as a ligand during Pd catalysis led to reasonable preparative yields of 50% when the reaction was run overnight at 120 °C. Pd catalysis with X-Phos was attempted under similar conditions (120 °C overnight), which led to 8% yield of TPz−Et and complete consumption of starting materials. Shortening the reaction time to 2 h gave a 68% yield with X-Phos. Longer reaction times seemed to be necessary when arylated and ester groups were incorporated onto the TPz building block potentially due to deactivation of the thiophene to nucleophilic attack on a Br−Pd−TPA catalytic intermediate.[44,45] The withdrawn nature of these substituents relative to the ethyl substituents is outlined in the UV−vis section below. All dyes were available just in four synthetic steps in up to 22% overall yield.

UV−Vis−NIR Absorbance and Electrochemical Properties. The optical and electrochemical properties of each of the TPz D−A−D dyes were analyzed to evaluate the effect of R-group substituents on absorption range, optical band gap size, and the potential of the products to function as NIR emissive materials. The TPz D−A−D dye λ_{max} ranged broadly from 530 to 665 nm as an apparent single, broad intramolecular charge transfer (ICT) transition. The simple ethyl alkyl chain shows the highest energy absorption (TPz−Et) and the direct ester substituted group shows the lowest energy absorption (TPz−CO_2Et, Figure 2, Table 1). The λ_{onset} values ranged from 650 nm for TPz−Et to 830 nm for TPz−CO_2Et with broad absorptions extending substantially into the NIR range for these D−A−D dyes.

Scheme 1. Synthetic Scheme for TPz−Et, TPz−CO_2Et, TPz−Ph, TPz−PhOMe, and TPz−$PhCO_2$Me[a]

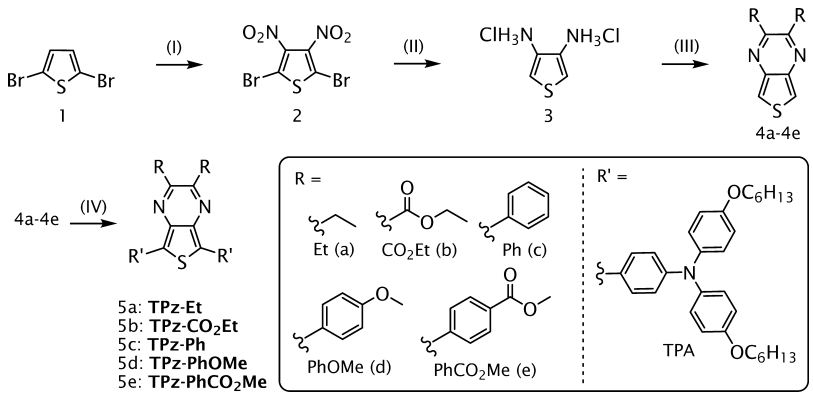

[a]Reagents and conditions: (I) Conc. H_2SO_4 (2.4 M), fuming H_2SO_4 (1.55 M), conc. HNO_3 (2.83 M), 2,5-dibromothiophene, room temperature, 3 h, 52%. (II) Conc. HCl (0.16 M), Sn powder (7.0 equiv), room temperature, 2 h, 75%. (III) For **4a**, **4b**, **4c**, and **4e**, triethylamine (0.2 M), dichloromethane (0.11 M), ethanol (0.11 M), dione (1.02 equiv, 3,4-hexanedione, benzil, diethyl 2,3-dioxosuccinate, dimethyl 4,4′-oxalyldibenzoate), 50 °C, overnight, giving yields of 82% (**4a**), 34% (**4b**), 45% (**4c**), and 85% (**4e**). For **4d**, 4,4′-dimethoxybenzil (1.0 equiv), methanol (0.2 M), $SnCl_2/SiO_2$ (5% w/w), room temperature, 2.5 h, 44% yield. (IV) For TPz−Et, 4-bromo-*N*,*N*-bis(4-hexyloxyphenyl)aniline (TPA-Br, 2.0 equiv), P(tBu)$_3$ (5 mol %), K_2CO_3 (1.5 equiv), Pd(OAc)$_2$ (5%), pivalic acid (0.5 equiv), toluene (0.25 M), 120 °C, overnight, 50% (TPz−Et) *or* TPA-Br (2 equiv), X-Phos (0.1 equiv), Cs_2CO_3 (2 equiv), Pd(OAc)$_2$ (5 mol %), toluene (0.5 M), 120 °C, 2 h, 68% yield. For TPz−CO_2Et, TPz-Ph, TPz-PhOMe and TPz-$PhCO_2$Me: TPA-Br (2 equiv), X-Phos (0.1 equiv.), Cs_2CO_3 (2 equiv), Pd(OAc)$_2$ (5 mol%), toluene (0.5 M), 120°C, overnight, 34% (TPz-CO_2Et), 40% (TPz-Ph); 50% (TPz-PhOMe); 65% (TPz-$PhCO_2$Me).

DOI: 10.1021/acs.joc.5b01958
J. Org. Chem. 2016, 81, 32−42

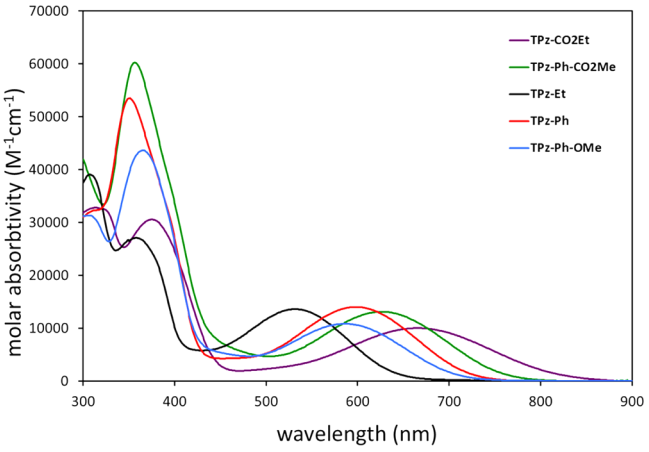

Figure 2. Absorption curves of TPz−Et (black), TPz−CO_2Et (purple), TPz−Ph (red), TPz−PhOMe (blue), and TPz−PhCO_2Me (green) in dichloromethane.

A clear optical band gap response can be seen as the absorption curve onset shifts toward lower energy with increased electron withdrawing group strength for the aryl-substituted dyes as TPz−PhOMe < TPz−Ph < TPz−PhCO_2Me. Accordingly, strongly donating substituents on the pyrazine ring of the TPz led to a hypsochromic shift in absorptions, with TPz−Et showing the highest energy ICT band. The strongest electron withdrawn substituted pyrazine ring (the two directly substituted esters of TPz−CO_2Et) led to the largest bathochromic shift in the series. We interpret these results as increasing the electron-withdrawing nature on the most electron deficient region of the TPz molecule, the pyrazine ring, which strengthens ICT through more complete charge transfer from the most electron rich TPA region. The converse of this is empirically observed as well in that if additional donating groups are installed directly on the pyrazine ring (TPz−Et or TPz−PhOMe) the ICT band shifts to higher energy by reducing the extent of charge transfer through a weakening of the acceptor region strength. All dyes had relatively similar molar absorptivities ranging from 14 000 to 10 000 M^{-1} cm^{-1} in chlorinated solvent.

The electrochemical properties of the dyes were evaluated as these are critical for a number of applications involving NIR small-molecule dyes, including solar cells, display applications, and photochemical reactions, and for assessing of the stability of these materials under ambient atmosphere. The dye ground-state oxidation potentials ($E_{(S+/S)}$) closely ranged from 0.71 to 0.78 V versus normal hydrogen electrode (NHE) in the following order for the TPz substituents: Ph < PhOMe = PhCO_2Me < Et < CO_2Et [Table S1 of the Supporting Information (SI), Figure 3]. This order indicates that the substituents on the pyrazine ring modestly contribute to the ground-state oxidation potential

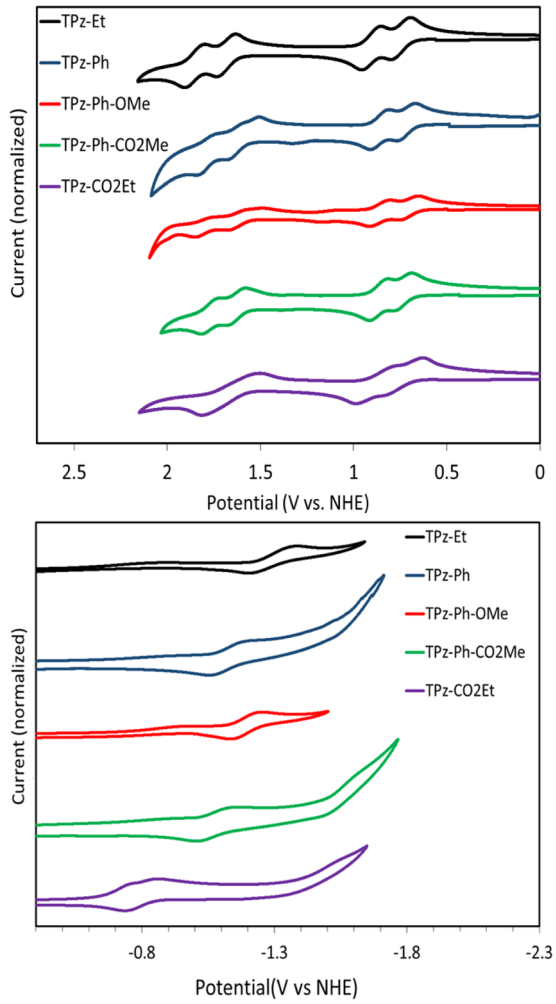

Figure 3. Cyclic voltammetry curves for oxidation (top) and reduction (bottom) of TPz−Et (black), TPz−PhOMe (blue), TPz−Ph (red), TPz−PhCO_2Me (green,) and TPz−CO_2Et (purple) in dichloromethane.

energies of electrons in the conjugated π-system, as the values are weakly tunable based on group choice. However, the excited-state oxidation potentials ($E_{(S+/S^*)}$, calculated from the equation $E_{(S+/S^*)} = E_{(S+/S)} - E_g^{opt}$, where $E_g^{opt} = 1240/\lambda_{onset}$) varied substantially on the basis of TPz substituent choice from −1.17 to −0.71 V, indicating that the substituents have a strong control on $E_{(S+/S^*)}$ values and the optical band gap as $E_{(S+/S)}$ values are relatively unchanging. The oxidation potential measurements show minimal variation over a 0.71−0.75 V range. It is also noteworthy that four reversible oxidation potentials were observed for each of the dyes examined

Table 1. UV−Vis−NIR Absorbance and Electrochemical Data

dye (TPz−R)	λ_{max} (nm)[a]	λ_{onset} (nm)[b]	λ_{emis} (nm)	Stokes shift (nm, eV)	ε ($M^{-1}cm^{-1}$)[a]	E_g^{opt} (eV)[c]	$E_{(0-0)}$ (eV)	$E_{(S+/S^*)}$ (V)[d]
Et	532	650	725	193, 0.62	13 600	1.91	1.95	−1.17
CO_2Et	665	830	–	–	12 000	1.49	–	−0.71
Ph	600	725	793	193, 0.50	14 000	1.71	1.78	−1.00
PhOMe	590	720	752	162, 0.45	11 100	1.72	1.81	−0.99
PhCO_2Me	626	770	820	194, 0.47	13 100	1.61	1.70	−0.88

[a]Measured in dichloromethane (DCM). [b]The absorption onset (λ_{onset}) was taken at the intercept of a tangent line on the low energy side of the λ_{max} peak and the *X*-axis. [c]E_g^{opt} was found through the equation $E_g^{opt} = 1240/\lambda_{onset}$. [d]$E_{(S+/S^*)}$ was calculated using $E_{(S+/S^*)} = E_{(S+/S)} - E_g^{opt}$.[46−48] $E_{(0-0)}$ was taken as the intercept of the absorption and emission curves.

DOI: 10.1021/acs.joc.5b01958
J. Org. Chem. 2016, 81, 32−42

(see Table S1 of the SI,Figure 3, top). In stark contrast to the oxidation potential measurements, the reduction potentials show a more dramatic range of potentials (−0.80 to −1.30 V), indicating a significant influence of the pyrazine ring substituents on the energy at which the TPz−TPA dyes accept electron density. The lowest energy reduction potential was observed for TPz−CO_2Et dye with the directly substituted esters on the pyrazine ring. The highest energy ground-state reduction potential was observed for TPz−Et and the dyes generally followed a trend with the most electron deficient substituents leading to the lowest energy reduction potentials (TPz−CO_2Et < TPz−PhCO_2Me < TPz−Ph < TPz−PhOMe < TPz−Et). Only a single reduction potential was observed for these dyes. These materials offer the attractive possibility of tuning $E_{(S+/S^*)}$ values while holding $E_{(S+/S)}$ values constant, which dramatically simplifies the controllable modification of dye energetics for various applications. The alkyl-substituted TPz−Et was found to have the highest energy $E_{(S+/S^*)}$ value (−1.17). Neutral and electron-rich aryl-substituted TPz dyes, TPz−Ph and TPz−PhOMe, demonstrated similar $E_{(S+/S^*)}$ values at −1.00 V, which is significantly stabilized (170 mV) when compared with the alkyl-substituted TPz dye. Addition of electron-deficient aryl groups and directly substituted esters on the TPz bridge gave substantially stabilized $E_{(S+/S^*)}$ values of −0.88 and −0.71 V. The possibility of tuning excited-state potentials by 460 mV with only slight modification to the ground-state potentials by 60 mV or less illustrates the straightforward tunability of these materials for a host of potential applications.

Computational Results. Density functional theory (DFT) and time-dependent density functional theory (TD-DFT) computational studies were undertaken to evaluate the orbital arrangement (Figure 4) of these dyes, to determine the orbitals involved in the broad absorption spectrum, and to confirm the ICT nature of the broad absorption band in the UV−vis−NIR spectrum. The geometries of these dyes were first optimized with the B3LYP functional and 6-311G(d,p) basis set (Figure 4, Table 2). The TPz−TPA dihedral bond angle (Figure 5) was found to be similar for all the dyes near 20°. Interestingly, TPz−CO_2Et optimized to a nonsymmetric structure with one TPA group giving a more planarized TPz−TPA bond of 13° and the other a value near 20°. The dihedral angle between the TPz−R substituents was similar for all the aryl substituents at ∼40°, regardless of donating or withdrawing substituent. TPz−CO_2Et again gave a dissymmetric structure with regard to bond angle at the TPz−ester bond, with one group showing a 29° angle and the second showing a 50° bond angle. The lower bond angles were on opposite sides of the TPz bridge, indicating a significant electronic communication from the donor across the TPz bridge to an opposite acceptor. It is noteworthy that a simple valence bond theory drawing does not allow for a charge-separated resonance structure involving these two substituents. The highest occupied molecular orbital (HOMO) and lowest unoccupied molecular orbital (LUMO) arrangements are plotted in Figure 3. In all cases, the HOMO is predominately localized on the TPA donor group with the LUMO localized on the TPz acceptor group. With a moderate iso value of 0.4 only the directly substituted ester group of TPz−CO_2Et demonstrated any appreciable LUMO localization onto the pyrazine substituents.

TD-DFT analysis with the B3LYP functional and 6-311G(d,p) basis set was preformed to analyze the predicted 10 lowest vertical transition energies in vacuum and to identify the contributing orbitals to the absorption bands observed. The lowest-energy vertical transition trends are in good agreement with the UV−vis−NIR experimental λ_{max} data trends, giving the following order for dyes from high to low eV energy: TPz−Et > TPz−PhOMe > TPz−Ph > TPz−PhCO_2Me > TPz−CO_2Et. The oscillator strength predictions indicate roughly similar vertical transition energy strengths, which is in good agreement with the experimental molar absorptivity measurements. The

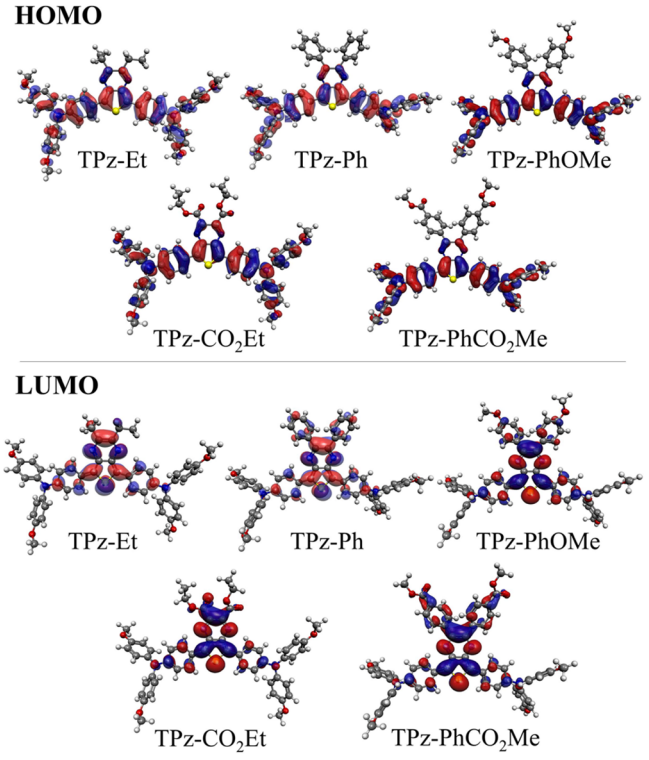

Figure 4. HOMO (top) and LUMO (bottom) orbitals of TPz−Et, TPz−CO_2Et, TPz−Ph, TPz−PhOMe, and TPz−PhCO_2Me. Iso values were set to 0.3.

Table 2. Computational Results from DFT and TD-DFT Analysis

dye	vert. trans. (nm, eV)	oscillator strength	angle 1 (deg)	angle 2 (deg)
TPz−Et	640, 1.94	0.59	19	–
TPz−CO_2Et	781, 1.59	0.43	13, 18	29, 50
TPz−Ph	706, 1.76	0.41	20	41
TPz−PhOMe	683, 1.82	0.42	20	39
TPz−PhCO_2Me	755, 1.64	0.33	21	41

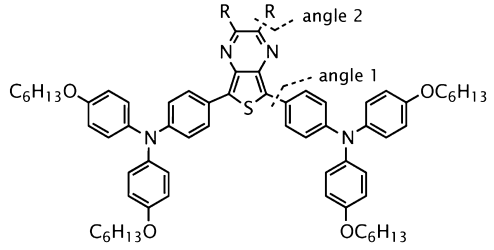

Figure 5. Graphical representation of the TPz−TPA dihedral angle (angle 1) and of the TPz−R substituent dihedral angle (angle 2) for the TPz D−A−D dyes.

DOI: 10.1021/acs.joc.5b01958
J. Org. Chem. 2016, 81, 32−42

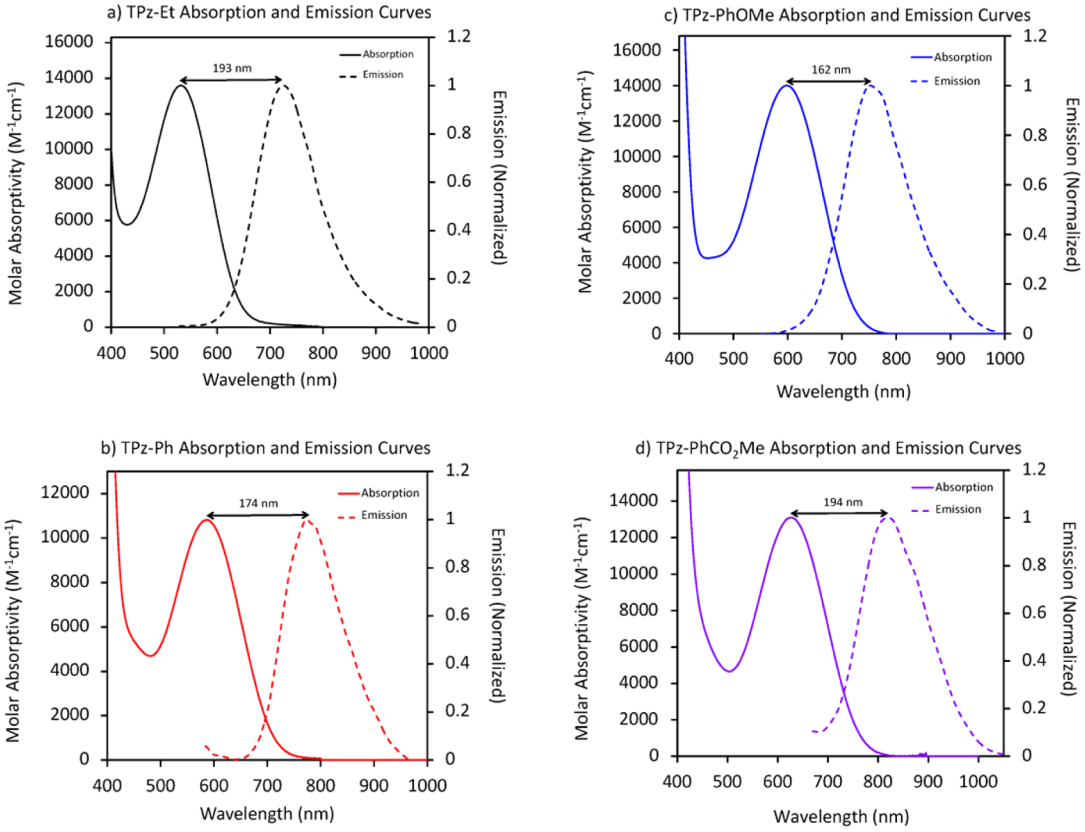

Figure 6. Absorbance and fluorescence spectrum of (a) TPz−Et, (b) TPz−Ph, (c) TPz−PhOMe, and (d) TPz−$PhCO_2Me$ in $CHCl_3$.

lowest-energy vertical transitions were all dominated by the HOMO−LUMO transitions (>99%), with the next nearest transitions being >100 nm higher in energy. The NIR absorptions of these dyes are attributed to strong ICT events based on the frontier molecular orbital arrangements of these dyes and the high percent contribution of the HOMO−LUMO transition to the low-energy vertical transition.

Emissive Properties. The emissive properties of the dyes were evaluated in solution, bulk solid, and single-molecule films. The fluorescence spectra of compounds **1**−**5** were recorded in $CHCl_3$, DMF, and MeOH/$CHCl_3$ (Figure 6). For applications requiring significant separation of input energy versus output energy, such as live fluorescence imaging, a large Stokes shift (>100 nm) is desirable to allow for significant energetic separation of the excitation source and emitted energy detected to avoid background signal detection. For this application specifically, ideally molecules should absorb and emit within the therapeutic window ranging from ∼650 to 1100 nm depending on the targeted tissue region. All dyes except TPz−Et have appreciable absorptions within the desired regions, and Stokes shifts of 162−194 nm were observed throughout the series (Table 1). The largest shifts were observed for TPz−Et and TPz−$PhCO_2Me$ with Stokes shifts near 200 nm. The observed large Stokes shifts are likely in part due to a geometric reorganization in the excited-state to allow for planarization of the TPz substituents (discussion below). TPz−CO_2Et was found to be nonemissive, which may be attributed to a substantially lower energy absorption leading to thermal energy loss as the energy-gap law suggests.

A solvatochromism study was performed on TPz−Ph in order to elucidate the nature of the intramolecular charge transfer state. The results reveal the clear trend of an increased Stokes shift as solvent polarity increases (Figure S1, SI). The absorption maximum is relatively unaffected by solvent polarity while the emission maximum ranges from 748 to 806 nm, suggesting that the geometry of the excited state is sensitive to solvent effects. The results can be seen in Figure 7 and are summarized in Table 3.

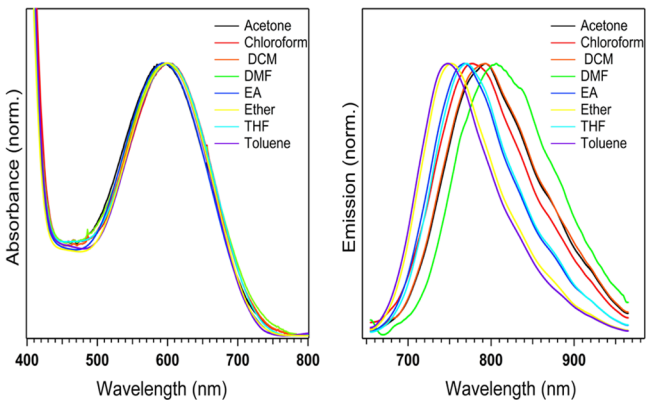

Figure 7. Absorption (left) and emission (right) spectra of TPz−Ph in different solvents.

To better understand the origin of these large Stokes shifts, computational analysis of the ground-state geometry, excited-state geometry, and vertical transitions were undertaken through DFT and TD-DFT [B3LYP/6-311G(d,p)] methods (Figure 8). Since the Franck−Condon principle teaches that electrons move faster than atomic nuclei, the first vertical excitations should occur in the absence of atom nuclei movements (Figure 8). After excitation, atomic nucleus reorganization may occur to give

DOI: 10.1021/acs.joc.5b01958
J. Org. Chem. 2016, 81, 32−42

Table 3. Results of Solvatochromism Study on TPz−Ph

solvent	absorption max. (nm)	emission max. (nm)	Stokes shift (nm, eV)
toluene	600	748	148, 0.41
ether	600	751	151, 0.42
THF	601	770	169, 0.45
EA	594	768	174, 0.47
chloroform	601	777	176, 0.47
DCM	598	793	195, 0.51
acetone	592	793	201, 0.53
DMF	598	806	208, 0.54

a lower-energy excited-state geometry (ΔS_1 geometry) prior to energy loss through emission, where again atomic nucleus reorganization is slower than electronic state changes. After emission, the excited-state geometry is accessed in the S_0 state, which then relaxes to the ground-state geometry (ΔS_0 geometry). The difference in the two electronic transitions yields the sum of the ΔS_1 and ΔS_0 geometries. This energy represents the reorganization energy of the molecule or the Stokes shift. We employed the following operations to better understand the observed Stokes shifts: (1) optimization of the ground-state geometry, (2) vertical excitation of electrons in this geometry (absorption), (3) optimization of the excited-state geometry, and (4) vertical excitation of electrons in the excited-state geometry (emission). Computational analysis of TPz−Ph shows a vertical excitation of the ground-state geometry at 706 nm (1.76 eV) and a vertical excitation of the excited-state geometry at 913 nm (1.36 eV) for a difference of 0.40 eV. This value is in good agreement with the experimental value for the difference in absorption and emission maximums (0.46 eV). Having found a reasonable agreement between experimental and computational values for the magnitude of energy of the Stokes shifts, we then analyzed the geometry to better understand where the atomic nuclei geometries were changing. Through dihedral bond angle analysis we found that in the ground-state geometry the TPz−TPA bond angle is 20°, whereas in the excited-state geometry the TPz−TPA bond angle is only 3°. This result is supported by the solvachromatic studies, where highly polar solvents promoting charge transfer led to larger Stokes shifts and presumably more planar excited-state geometries (Figure 7). This significant change in bond angle geometry between the TPA donor and TPz acceptor was found to be the largest contributor to the reorganization energy. The remaining bond angles are nearly unchanged. This analysis provides a method for rationally controlling the Stokes shift magnitude through steric modifications near the TPA−TPz bond.

The fluorescence quantum yield (QY) is an important parameter in the evaluation of emissive materials, as a high QY is desirable for an accurate detection of dyes in low concentration and for low-power-consumption devices. All dyes were tested in three solvent systems, including DMF, $CHCl_3$ and a MeOH−$CHCl_3$ mixture, under both a nitrogen atmosphere and under ambient conditions. DMF was selected to evaluate the effects of a polar aprotic solvent, $CHCl_3$ was selected to evaluate the effects of a relatively low polarity solvent, and MeOH−$CHCl_3$ was selected as a polar protic solvent system, as the dyes were not highly soluble in pure MeOH. Ideally, for biologically related imaging, the dyes should emit strongly in protic environments. The QYs of the TPz−Ph and TPz−PhOMe dyes are comparable to widely used NIR dyes with emission peaks in the 700−800 nm region, such as cyanines,[49] benzothiadiazoles,[50] and benzothiophenes.[51] TPz−Et, TPz−Ph, TPz−PhOMe, and TPz−$PhCO_2Me$ were found to give QYs ranging from 0.3% to 4.3% in various environments. All dyes were found to have higher quantum yields under nitrogen rather than under ambient conditions; however, the percent decrease in quantum yield varied dramatically from a 4% decrease for TPz−Et in $CHCl_3$ to an 80% decrease for TPz−PhOMe when in DMF. TPz−Ph gave the highest QY of 4.3% in $CHCl_3$ under a nitrogen atmosphere. In general, $CHCl_3$ and MeOH−$CHCl_3$ mixtures were minimally affected by ambient atmospheric conditions, while DMF solutions were much more strongly affected. Under the best conditions tested, the trend in maximum QY proceeded as TPz−$PhCO_2Me$ (0.26%) < TPz−Et (2.3%) < TPz−PhOMe (2.9%) < TPz−Ph (4.3%). It is noteworthy that despite a ∼75 nm lower energy absorption, TPz−Ph demonstrated a nearly 2-fold increase in QY when compared with TPz−Et. This is likely in part due to a reduced Stokes shift, as a lower reorganization energy is needed to access the excited state, resulting in a higher emission energy and better intermolecular spacing of the conjugated electrons through out-of-plane phenyl spacers versus ethyl groups. TPz−Ph also demonstrated the higher QY in a protic environment of 3.7%, which is nearly an order of magnitude (8 times) higher than for the next highest performing dye in this environment. The full solvent and atmospheric dependence of the QY is shown in Table 4.

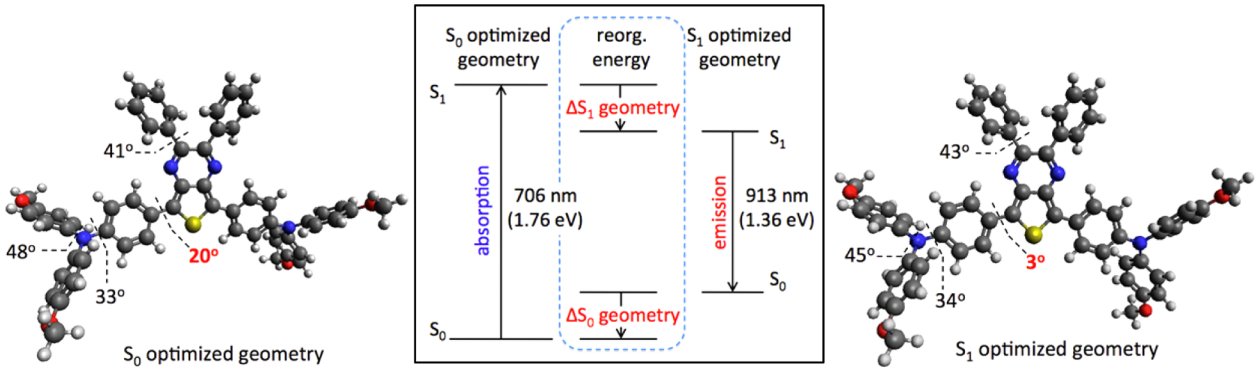

Figure 8. Computational analysis of the ground-state (left) and excited-state (right) geometries for TPz−Ph through DFT analysis at the B3LYP/6-311G(d,p) level. An energetic diagram illustrating results from TD-DFT [B3LYP/6-311G(d,p)] analysis of both the S_0 and S_1 geometries is provided as the center figure. The energetic difference in the two vertical excitations (absorption and emission) is shown as the reorganization energy and is the sum of the ΔS_0 geometry and the ΔS_1 geometries.

DOI: 10.1021/acs.joc.5b01958
J. Org. Chem. 2016, 81, 32−42

Table 4. Emissive Properties

dye	solvent	QY(φ) (%)	τ_1 (ns)	τ_2 (ns)
TPz−Et	DMF[a]	1.63	0.85	N/A[c]
	DMF[b]	2.05	0.92	N/A
	$CHCl_3$[a]	2.16	1.12	N/A
	$CHCl_3$[b]	2.25	1.09	N/A
	MeOH−$CHCl_3$[a]	0.36	0.41	0.41
	MeOH−$CHCl_3$[b]	0.45	0.52	0.52
TPz−Ph	DMF[a]	2.13	0.44	14.58
	DMF[b]	3.29	0.65	13.68
	$CHCl_3$[a]	3.51	1.22	11.42
	$CHCl_3$[b]	4.29	1.23	13.04
	MeOH/$CHCl_3$[a]	2.62	0.85	4.46
	MeOH−$CHCl_3$[b]	3.74	1.02	7.11
TPz−PhOMe	DMF[a]	0.56	0.50	N/A
	DMF[b]	2.87	0.57	N/A
	$CHCl_3$[a]	0.86	0.68	3.34
	$CHCl_3$[b]	1.40	0.75	4.06
	MeOH−$CHCl_3$[a]	0.34	0.55	N/A
	MeOH−$CHCl_3$[b]	0.41	0.55	N/A
TPz−$PhCO_2Me$	DMF[a]	0.15	0.54	N/A
	DMF[b]	0.21	0.61	N/A
	$CHCl_3$[a]	0.21	0.51	N/A
	$CHCl_3$[b]	0.26	0.58	N/A
	MeOH−$CHCl_3$[a]	0.08	0.60	N/A
	MeOH−$CHCl_3$[b]	0.12	0.63	N/A

[a]Readings were taken in solvents under ambient conditions. [b]Readings were taken in N_2-degassed solvents. [c]N/A = not applicable.

Fluorescence lifetimes (τ) of compounds **1**−**3** were also measured, as the QY is related to fluorescence lifetimes by the equations $\varphi = k_r/(k_r + k_{nr})$, where k_r is the radiative rate and k_{nr} is the nonradiative rate, and $\tau = 1/(k_r + k_{nr})$, which gives $\varphi = \tau k_r$. While a large τ does not necessitate a higher φ, as k_r is independent, increasing τ often correlates to higher φ. TPz−Ph showed a significantly longer lifetime than the other dyes. Interestingly, TPz−Ph was observed to have a two-component decay curve, with a fast component at ∼1 ns for each solvent/atmosphere and a substantially longer excited-state-decay component lasting approximately an order of magnitude longer than the fast component. Only the pyrazine−arylated-TPz acceptors gave significant two-component fluorescence lifetimes. For all dyes, the initial τ_1 ranged between ∼0.5 and 1.0 ns in all solvents and atmospheres analyzed. The solvent dependence of the fluorescent lifetimes is shown in Table 4 for the full dye series.

Since TPz−Ph was found to have the highest QY with emission into the NIR region, solid-state measurements with thin film fluorescence measurements were taken (Figure 9). Standard thin films of TPz−Ph display emission spectra comparable to solution-phase samples, suggesting a limited aggregative interaction between the dye molecules in the solid state. However, the thin film emission spectrum of TPz−Ph does not show the same degree of red shifting observed in solution phase. This indicates that the molecules are more tightly packed in the films than in solution, inhibiting reorganization. Zeonex films allow for the direct observation of single molecule emission in the solid-state through dissolving of the emissive material in a solution of Zeonex and casting films.[52] These studies allow for the direct observation of the stability of a single molecule to continuous irradiation and

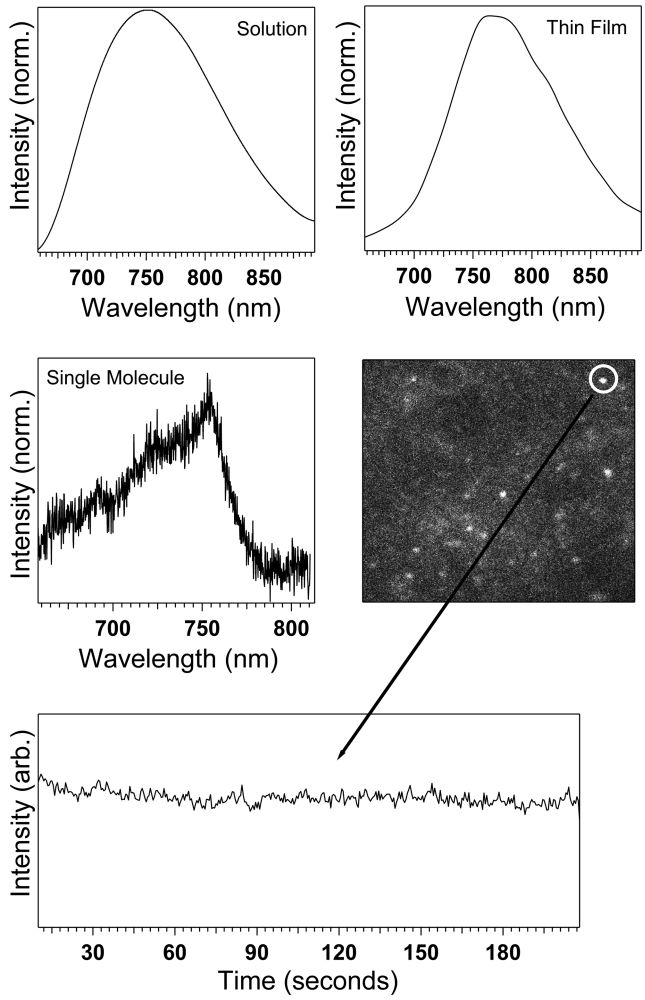

Figure 9. Fluorescence spectrum of TPz−Ph in DMF (upper left), as a neat thin film on a glass slide (upper right), and dispersed in a Zeonex thin film (middle), and the accumulated spectrum of approximately 20 single molecules dispersed in a solid Zeonex film (bottom).

emission. Spectra of ultradispersed single molecules in a solid Zeonex film display a similar emission λ_{max} to the more concentrated thin film, but λ_{max} does not tail as far into the longer-wavelength region. A fluorescence time trace of a single molecule of TPz−Ph is shown in Figure 9, demonstrating that the emission of a single molecule in the Zeonex film is stable with continuous fluorescence.

■ CONCLUSION

A series of four NIR fluorescent compounds, with emission ranging from 600 to 900 nm, were synthesized and the optical properties studied. The facile four-step synthesis was made possible through direct C−H bond arylation with catalytic palladium. The NIR dyes were analyzed with electrochemical studies, UV−vis spectroscopy, and fluorometry in a variety of solutions, as a thin film and at the solid-state single-molecule level in Zeonex films. These materials were shown to have near independently tunable ground-state and excited-state oxidation potentials, which give rise to the opportunity to control and tune energy values in a straightforward manner. Solution absorption and emission curves show Stokes shifts near 200 nm for the TPA−TPz−TPA (D−A−D) dyes. The Stokes shift origin was examined through computational analysis and found

DOI: 10.1021/acs.joc.5b01958
J. Org. Chem. 2016, 81, 32−42

to correlate with a substantial bond angle change between the donor and acceptor rings. Good quantum yields near that of commonly used biological imaging dyes, such as cyanine dyes, are observed at >4% in the NIR region (~775 nm peak emission), despite a considerable enhancement in Stokes shift values (200 vs ~5 nm). Large Stokes shifts are desirable for living biological imaging applications to avoid background signals from the excitation source, and the TPz-based dyes examined have demonstrated a large shift and good emission quantum yield. The emission of these materials was shown to be stable in a solid film during irradiation, which suggests that the molecules are part of a robust design with potential applications in a range of devices.

EXPERIMENTAL SECTION

Materials. All commercially obtained reagents and solvents were used as received without further purification. 2,5-Dibromothiophene, benzil, 4,4′-dimethozybenzil, 3,4-hexanedione, and methyl 4-formylbenzoate were purchased commercially. Bis(hexyloxy)triphenylamine bromide was prepared according to literature procedures.[53] Diethyl 2,3-dioxosuccinate,[54] dimethyl 4,4′-oxalyldibenzoate,[55] and the $SnCl_2$/SiO_2 solid support catalyst[43] were prepared according to literature procedures. Thin-layer chromatography (TLC) was visualized with UV. Flash column chromatography was performed as described by Still.[56] ^1H and ^{13}C NMR spectra were recorded on 300 and 500 MHz spectrometers and are reported in ppm using solvent as an internal standard ($CDCl_3$ at 7.26 ppm). Data are reported as s = singlet, d = doublet, t = triplet, q = quartet, p = pentet, m = multiplet, b = broad, ap = apparent, dd = doublet of doublets, and coupling constant(s) are in hertz, followed by integration information. UV−vis spectra were measured with a UV−Vis−NIR spectrometer. Cyclic voltammetry was measured with a electrochemical analyzer. Compounds **2**−**4c** are known compounds referenced below with a brief description of the preparative methods used and matching ^1H NMR data reported. During NMR sample preparation, we found extraction with dichloromethane and aqueous $NaHCO_3$ was necessary for resolved signals after silica gel purification. Presumably these compounds tightly cling to trace SiO_2 particles, leading to poorly resolved NMR peaks, and aqueous extraction allows for separation of these particles. HRMS spectra were obtained with a QTOF HRMS utilizing nanospray ionization. The mass analyzer was set to the 100−2000 Da range.

Synthesis of 2,5-Dibromo-3,4-dinitrothiophene (2).[40] To a flame-dried, round-bottom flask were added concentrated H_2SO_4 (25.00 mL, 2.40 M), concentrated HNO_3 (22 mL, 2.83 M), and fuming H_2SO_4 (40 mL, 1.55 M). The flask was then cooled to 0 °C, followed by addition of 2,5-dibromothiophene (6.98 mL, 62.0 mmol) dropwise at a rate that kept the temperature below 15 °C. After complete addition, the reaction mixture was then stirred for 3 h at room temperature. The reaction mixture was poured into a 300 g of crushed ice; while the ice was melting, the yellow precipitate was collected by vacuum filtration. The product was purified through recrystallization with methanol to give a yellow color crystalline solid (10.70 g, 52.0%): ^{13}C NMR (500 MHz, d_6-DMSO) δ 140.2, 117.1 ppm.

Synthesis of 3,4-Diaminothiophene Dihydrochloride (3).[40] To a flame-dried flask were added concentrated HCl (146 mL, 37%) and **2** (8.00 g, 24.10 mmol). The flask was then cooled to 0 °C followed by addition of Sn powder (20.15 g, 169.90 mmol) within one hour in small portions to keep the temperature below 25 °C. After complete addition, the mixture was stirred at room temperature until all the Sn was consumed (2 h). After cooling for 1 h in a −18 °C refrigerator, the product was collected by vacuum filtration and washed with diethyl ether and acetonitrile to give a white powder (3.39 g, 75%). The product was used as isolated without further characterization.

Synthesis of 2,3-Diethylthieno[3,4-*b*]pyrazine (4a).[42] A mixture of 3,4-diaminothiophene dihydrochloride (**3**) (1.00 g, 5.35 mmol), 3,4-hexanedione (0.67 mL, 5.46 mmol), triethylamine (27 mL), ethanol (49 mL), and dichloromethane (49 mL) was stirred at 50 °C overnight under ambient atmosphere. The reaction mixture was extracted with dichloromethane and dried over $MgSO_4$. The crude product was purified by flash silica gel chromatography with 10% ethyl acetate:dichloromethane → 30% ethyl acetate:dichloromethane as the eluent to give tan crystalline solid (0.85 g, 82.4%): ^1H NMR (300 MHz, $CDCl_3$) δ 7.81 (s, 2H) 2.95 (q, J = 7.4 Hz, 4H), 1.38 (t, J = 7.4 Hz, 6H).

Synthesis of Diethyl Thieno[3,4-*b*]pyrazine-2,3-dicarboxylate (4b):[41] The synthetic procedure is similar to the conditions for **4a**, except diethyl 2,3-dioxosuccinate (excess, estimated 4 equiv) was used instead of 3,4-hexanedione. The crude product was purified through a silica gel plug using 100% dichloromethane → 10% ethyl acetate:dichloromethane to give a tan solid (155 mg, 34%): ^1H NMR (300 MHz, $CDCl_3$) δ 8.29 (s, 2H), 4.54 (q, J = 7.1 Hz, 4H), 1.47 (t, J = 7.1 Hz, 6H).

Synthesis of 2,3-Diphenylthieno[3,4-*b*]pyrazine (4c):[36] The synthetic procedure is similar to the conditions for **4a**, except benzil (1.15 g, 5.45 mmol) was use instead of 3,4-hexanedione. The crude product was purified through silica gel chromatography with 100% dichloromethane → 5% ethyl acetate:dichloromethane as the eluent to give a tan crystalline solid (0.69 g, 45%): ^1H NMR (300 MHz, $CDCl_3$) δ 8.05 (s, 1H), 7.44 (dd, J = 2.2, 7.7 Hz, 4H), 7.36−7.30 (m, 6H).

Synthesis of 2,3-Bis(4-methoxyphenyl)thieno[3,4-*b*]pyrazine (4d). To a flame-dried, N_2-filled round-bottom flask was added 3,4-diaminothiophene dihydrochloride (**3**) (0.50 g, 2.67 mmol), 4,4′-dimethoxybenzil (0.66 g, 2.43 mmol), $SnCl_2/SiO_2$ (0.72 g, 0.12 mmol), and methanol (14 mL). The mixture was stirred at room temperature for 3 h. The reaction mixture was filtered through a thin pad of SiO_2 with 20% ethyl acetate:dichloromethane. The filtrate was then concentrated and purified through flash silica gel chromatography with 5% ethyl acetate:dichloromethane → 10% ethyl acetate:dichloromethane to give a pale green color solid (0.37 g, 43.5%): ^1H NMR (300 MHz, $CDCl_3$) δ 7.97 (s, 2H), 7.40 (d, J = 8.6 Hz, 4H), 6.85 (d, J = 8.7 Hz, 4H), 3.83 (s, 6H); ^{13}C NMR (75 MHz, $CDCl_3$) δ 160.2, 153.0, 142.6, 131.8, 131.3, 117.0, 113.6, 55.3; IR (neat, cm^{-1}) 3435.1, 3066.4, 1635.6, 1606.2, 1248.7, 1173.4; HRMS (ESI) m/z calcd for $C_{20}H_{16}N_2O_2S$ (MH^+) 349.1011, found 349.0984.

Synthesis of Dimethyl 4,4′-(Thieno[3,4-*b*]pyrazine-2,3-diyl)dibenzoate (4e). The synthetic procedure is similar to the conditions for **4a**, except dimethyl 4,4′-oxalyldibenzoate (0.43 g, 1.31 mmol) was use instead of 3,4-hexanedione. The crude reaction mixture was purified through a silica gel column with 40% ethyl acetate:hexane → 100% methanol (0.40 g, 85%): ^1H NMR (500 MHz, $CDCl_3$) δ 8.11 (s, 2H), 7.98 (d, J = 7.9 Hz, 4H), 7.49 (d, J = 7.8 Hz, 4H), 3.92 (s, 6H); ^{13}C NMR (75 MHz, $CDCl_3$) δ 167.1, 152.4, 143.6, 142.0, 131.1, 129.8, 129.7, 118.5, 52.4; IR (neat, cm^{-1}) 3114.6, 1709.2, 1435.5, 1280.5, 1109.8; HRMS (ESI) m/z calcd for $C_{22}H_{16}N_2O_4S$ (M + H) 405.0909, found 405.0934.

Synthesis of 4,4′-(2,3-Diethylthieno[3,4-*b*]pyrazine-5,7-diyl)bis(*N*,*N*-bis(4-(hexyloxy)phenyl)aniline) (TPz−Et). To a vial cycled three times with high vacuum−N_2 and containing **4a** (40 mg, 0.21 mmol) was added 4-bromo-*N*,*N*-bis(4-hexyloxyphenyl)aniline (TPA-Br) (220 mg, 0.42 mmol), P(*t*-Bu)$_3$ (1 M in toluene) (11 μL, 0.012 mmol), K_2CO_3 (43 mg, 0.31 mmol), $Pd(OAc)_2$ (2.4 mg, 0.012 mmol), pivalic acid (11 mg, 0.10 mmol), and STS-dried toluene (1.5 mL) under a N_2 atmosphere. Then the vial was sealed and the reaction mixture was stirred at 120 °C for 3 h. The reaction mixture was filtered through a thin pad of Celite with dichloromethane. The filtrate was concentrated and purified by flash silica gel chromatography using 30% ethyl acetate:hexanes to give a purple solid (165 mg, 68%): ^1H NMR (500 MHz, $CDCl_3$) δ 8.10 (d, J = 8.7 Hz, 4H), 7.08 (d, J = 8.9 Hz, 8H), 6.98 (d, J = 8.8 Hz, 4H), 6.83 (d, J = 9.0 Hz, 8H), 3.94 (t, J = 7.2 Hz, 8H), 2.90 (q, J = 7.2 Hz, 4H), 1.81−1.75 (m, 8H), 1.40−1.36 (m, 8H), 1.39 (t, J = 7.3 Hz, 6H), 1.35−1.26 (m, 16H), 0.93−0.90 (m, 12H); ^{13}C NMR (125 MHz, $CDCl_3$) δ 155.6, 155.5, 147.9, 140.6, 138.3, 128.6, 128.0, 126.7, 126.1, 120.4, 115.3, 68.3, 31.6, 29.4, 28.2, 25.8, 22.7, 14.1, 11.3; IR (neat, cm^{-1}) 3849.5, 3746.4, 2921.7, 2859.8, 1503.1, 1235.0; HRMS (ESI) m/z calcd for $C_{70}H_{86}N_4O_4S$ (M^+) 1078.6370, found 1078.6378; mp 91.1 °C. Anal.

DOI: 10.1021/acs.joc.5b01958
J. Org. Chem. 2016, 81, 32−42

Calcd for $C_{70}H_{86}N_4O_4S$: C, 77.88%; H, 8.03%; N, 5.19%. Found: C, 78.15%; H, 8.03%; N, 5.02%.

Synthesis of Diethyl 5,7-Bis(4-(bis(4-(hexyloxy)phenyl)-amino)phenyl)thieno[3,4-*b*]pyrazine-2,3-dicarboxylate (TPz−CO_2Et). To a vial cycled three times with high vacuum−N_2 and containing **4b** (50 mg, 0.18 mmol) was added TPA-Br (190 mg, 0.37 mmol), X-Phos (17 mg, 0.035 mmol), Cs_2CO_3 (230 mg, 0.70 mmol), $Pd(OAc)_2$ (3.9 mg, 0.018 mmol), and STS-dried toluene (0.5 mL) under a N_2 atmosphere. The vial was sealed and the reaction mixture was stirred at 120 °C for overnight. Then the reaction mixture was filtered through a thin pad of Celite with dichloromethane. The filtrate was concentrated and purified by silica gel chromatography using 100% chloroform as the eluent to give a green solid (68 mg, 35%): ^{1}H NMR (300 MHz, $CDCl_3$) δ 7.98 (d, J = 8.9 Hz, 4H), 7.12 (d, J = 8.9 Hz, 8H), 6.99 (d, J = 8.9 Hz, 4H), 6.87 (d, J = 8.4, 8H), 4.48 (q, J = 7.1 Hz, 4H), 3.97 (t, J = 6.5 Hz, 8H), 1.60−1.58 (m, 8H), 1.43−1.37 (m, 8H), 1.36−1.30 (m, 6H), 1.27−1.24 (m, 16H), 0.93−0.90 (m, 12H); ^{13}C NMR (300 MHz, $CDCl_3$) δ 165.2, 156.1, 149.2, 142.4, 140.2, 136.8, 133.4, 128.7, 127.2, 124.4, 119.9, 115.5, 68.4, 62.4, 31.7, 29.5, 25.9, 22.8, 14.3, 14.2; IR (neat, cm^{-1}) 2927.4, 1720.7, 1597.4, 1502.3, 1468.4, 1234.8, 1150.0; HRMS (ESI) m/z calcd for $C_{72}H_{86}N_4O_8S$ (M^+) 1166.6166, found 1166.6169; mp 139.2 °C. Anal. Calcd for $C_{72}H_{86}N_4O_8S$: C, 74.07%; H, 7.42%; N, 4.80%. Found: C, 73.07%; H, 7.58%; N, 4.45%.

Synthesis of 4,4′-(2,3-Diphenylthieno[3,4-*b*]pyrazine-5,7-diyl)bis(*N*,*N*-bis(4-(hexyloxy)phenyl)aniline) (TPz−Ph). To a vial cycled three times with high vacuum−N_2 and containing **4c** (50 mg, 0.17 mmol) was added TPA-Br (180 mg, 0.35 mmol), X-Phos (8.3 mg, 0.017 mmol), Cs_2CO_3 (110 mg, 0.35 mmol), $Pd(OAc)_2$ (2.0 mg, 0.0087 mmol), and STS-dried toluene (1.5 mL) under a N_2 atmosphere. The vial was sealed and the reaction mixture was stirred at 120 °C for overnight. The reaction mixture was filtered through a thin pad of Celite with dichloromethane. The filtrate was concentrated and purified by flash silica gel chromatography using 50% dichloromethane:hexanes to give a purple solid (52 mg, 40.0%): ^{1}H NMR (500 MHz, $CDCl_3$) δ 8.10 (d, J = 8.8 Hz, 4H), 7.51 (d, J = 8.4 Hz, 4H), 7.33−7.26 (m, 6H), 7.11 (d, J = 8.9 Hz, 8H), 7.01 (d, J = 8.9 Hz, 4H), 6.85 (d, J = 9.0 Hz, 8H), 3.95 (t, J = 6.5 Hz, 8H), 1.82−1.77 (m, 8H), 1.55−1.51 (m, 8H), 1.38−1.28 (m, 16H), 0.94−0.85 (m, 12H); ^{13}C NMR (75 MHz, $CDCl_3$) δ 155.8, 151.9, 148.3, 140.5, 139.7, 138.1, 130.2, 130.0, 128.7, 128.4, 128.1, 127.1, 125.8, 120.4, 115.4, 68.4, 31.8, 29.5, 25.9, 22.8, 14.2; IR (neat, cm^{-1}) 2925.8, 2855.7, 1499.0, 1235.0; HRMS (ESI) m/z calcd for $C_{78}H_{86}N_4O_4S$ (M^+) 1174.6370, found 1174.6376; mp 128.3 °C. Anal. Calcd for $C_{78}H_{86}N_4O_4S$: C, 79.69%; H, 7.37%; N, 4.77%. Found: C, 78.84%; H, 7.46%; N, 4.71%.

Synthesis of 4,4′-(2,3-Bis(4-methoxyphenyl)thieno[3,4-*b*]-pyrazine-5,7-diyl)bis(*N*,*N*-bis(4-(hexyloxy)phenyl)aniline) (TPz−PhOMe). To a vial cycled three times with high vacuum−N_2 and containing **4d** (50 mg, 0.14 mmol) was added TPA-Br (150 mg, 0.30 mmol), X-Phos (6.8 mg, 0.014 mmol), Cs_2CO_3 (93 mg, 0.29 mmol), $Pd(OAc)_2$ (1.6 mg, 0.0072 mmol), and STS-dried toluene (1.5 mL) under an N_2 atmosphere. Then the vial was sealed and reaction mixture was stirred at 120 °C overnight. Then the reaction mixture was filtered through a thin pad of Celite with dichloromethane. The filtrate was concentrated and purified by silica gel chromatography using 50% dichloromethane:hexanes as the eluent to give a blue solid (51 mg, 50.0%). For a resolved ^{1}H NMR spectrum, addition of an aqueous base was necessary during data aquistion, potentially due to this molecule uniquely strongly binding to trace SiO_2 particles after column purification. Simple exctraction with a base after silica gel purification did not lead to resolved peaks. Due to the necessary addition of a base during NMR sample aquisition, an adiquate ^{13}C NMR spectrum could not be obtained due to the presence of a large base signal in the spectrum. Elemental analysis was conducted in place of this experiment to further characterize this compound: ^{1}H NMR (500 MHz, $CDCl_3$) δ 8.07 (d, J = 8.7 Hz, 4H), 7.47 (d, J = 8.7 Hz, 4H), 7.09 (d, J = 8.8 Hz, 8H), 6.99 (d, J = 8.7 Hz, 4H), 6.84−6.82 (m, 12H), 3.94 (t, J = 6.5 Hz, 8H), 3.82 (s, 6H), 1.81−1.75 (m, 8H), 1.36−1.35 (m, 8H), 1.25−1.20 (m, 16H), 0.92−0.90 (m, 12H); IR (neat, cm^{-1}) 2954.6, 2925.8, 2859.8, 1602.1, 1499.0, 1239.2; HRMS (ESI) m/z calcd for $C_{80}H_{90}N_4O_6S$ (M^+) 1243.6581, found 1234.6555; mp 111.6 °C. Anal. Calcd for $C_{80}H_{90}N_4O_6S$: C, 77.76%; H, 7.34%; N, 4.53%. Found: C, 77.25%; H, 7.67%; N, 3.98%.

Synthesis of Dimethyl 4,4′-(5,7-Bis(4-(bis(4-(hexyloxy)-phenyl)amino)phenyl)thieno[3,4-*b*]pyrazine-2,3-diyl)-dibenzoate (TPz−$PhCO_2$Me). The synthetic procedure follows the same procedure as TPz−Ph. The crude product was purified through flash silica gel chromatography using 6% ethyl acetate:hexanes to give a green solid (90 mg, 65%): ^{1}H NMR (500 MHz, $CDCl_3$) δ 8.05 (d, J = 8.3 Hz, 4H), 7.96 (d, J = 7.8 Hz, 4H), 7.55 (d, J = 7.9 Hz, 4H),7.09 (d, J = 7.7 Hz, 8H), 6.99 (d, J = 7.9, 4H), 6.84 (d, J = 8.2 Hz, 8H), 3.94 (t, J = 14.5 Hz, 14H), 1.85−1.74 (m, 8H), 1.60−1.43 (m, 8H), 1.42−1.25 (m, 16H), 0.99−0.86 (m, 12H); ^{13}C NMR (75 MHz, $CDCl_3$) 167.3, 156.1, 151.1, 148.7, 144.1, 140.4, 138.0, 131.2, 130.4, 130.0, 129.8, 128.7, 127.2, 125.5, 119.9, 115.5, 68.5, 52.0, 31.8, 29.5, 25.9, 22.8, 14.2; IR (neat, cm^{-1}) 2954.7, 2921.7, 2847.4, 1734.0, 1499.0, 1272.2; HRMS (ESI) m/z calcd for $C_{82}H_{90}N_4O_8S$ (M^+) 1290.6479, found 1290.6487; mp 157.0 °C. Anal. Calcd for $C_{80}H_{90}N_4O_6S$: C, 76.25%; H, 7.02%; N, 4.34%. Found: C, 76.18%; H, 7.07%; N, 4.13%.

Computational Analysis. MM2 energy minimization in Chem-Bio3D Ultra (version 13.0.2.3021) was used for the initial energy minimization of the TPz-based dyes. Dihedral angles for the relevant groups were set to values between the global minimum and the next local minimum on the conformational energy diagram as calculated by chemBio3D. Accurate geometry optimization was performed sequentially by density functional theory (DFT) using Guassian09[57] with the B3LYP[58,59] functional with the following basis sets: first 3-21G, second 6-31G(d,p), and finally 6-311G(d,p). Time-dependent density functional theory (TD-DFT) computations were performed with optimized geometries and with the B3LYP functional and 6-311G(d,p) basis set to compute the vertical transition energies and oscillator strengths.

Fluorescence Measurement Methods. Solution-phase fluorescent quantum yields were obtained using the optically dilute method described by Crosby and Demas.[60] All sample concentrations were on the order of 10^{-5} M to reduce reabsorption. The 514.5 nm line of an Ar^+ ion laser was used as the excitation source, and rhodamine B (φ = 0.31 in water)[61] and zinc phthalocyanine (φ = 0.30 in 1% pyridine in toluene)[62] were used as references. Fluorescent lifetimes were obtained by exciting with the 485 nm line of a pulsed diode laser (fwhm <100 ps) and detecting with a avalanche diode.

Polymer thin films were prepared by first dissolving the sample in spectroscopic grade cyclohexane. Once solutions were of sufficient concentration, Zeonex thin films were made by dissolving Zeonex pellets in the new dilute solution, one pellet per ∼2 mL of cyclohexane, followed by 20−30 min of sonication.[52] Plasma-cleaned capillary tubes with ∼100 μL of solution and the "drop and swipe" method were used to create Zeonex thin films on plasma-cleaned glass slides.

■ ASSOCIATED CONTENT

Supporting Information

The Supporting Information is available free of charge on the ACS Publications website at DOI: 10.1021/acs.joc.5b01958.

Electrochemical data, solvatochromism study, ^{1}H NMR and ^{13}C NMR spectra for all of the prepared compounds, and tables of computational data (PDF)

■ AUTHOR INFORMATION

Corresponding Authors

*J.H.D e-mail: delcamp@olemiss.edu.

*N.I.H. e-mail: nhammer@olemiss.edu.

Author Contributions

L.E.M and N.L. contributed equally to this work.

DOI: 10.1021/acs.joc.5b01958
J. Org. Chem. 2016, 81, 32−42

Notes

The authors declare no competing financial interest.

■ ACKNOWLEDGMENTS

N.I.H., L.E.M., J.H.D., N.L., A.P., and S.J.M. would like to gratefully acknowledge the NSF EPSCoR Program, Track I (EPS-0903787); the NSF EPSCoR Program, Track II (OIA-1539035); and the University of Mississippi for funding. S.J.M acknowledges the Ole Miss Physical Chemistry Summer Research Program NSF REU (CHE-1156713) and the Sally McDonnell Barksdale Honors College, and N.I.H. and L.E.M. acknowledge the National Science Foundation (CHE-0955550) for support. L.E.M. also acknowledges support from the U.S. Department of Education GAANN program (P200A120046).

■ REFERENCES

(1) Fabian, J.; Nakazumi, H.; Matsuoka, M. *Chem. Rev.* **1992**, *92* (6), 1197−1226.
(2) Mayerhöffer, U.; Deing, K.; Gruß, K.; Braunschweig, H.; Meerholz, K.; Würthner, F. *Angew. Chem., Int. Ed.* **2009**, *48* (46), 8776−8779.
(3) Qian, G.; Wang, Z. Y. *Chem. - Asian J.* **2010**, *5* (5), 1006−1029.
(4) Weil, T.; Vosch, T.; Hofkens, J.; Peneva, K.; Müllen, K. *Angew. Chem., Int. Ed.* **2010**, *49* (48), 9068−9093.
(5) Yao, L.; Zhang, S.; Wang, R.; Li, W.; Shen, F.; Yang, B.; Ma, Y. *Angew. Chem., Int. Ed.* **2014**, *53* (8), 2119−2123.
(6) Du, X.; Wang, Z. Y. *Chem. Commun.* **2011**, *47* (14), 4276−4278.
(7) Berezin, M. Y.; Achilefu, S. *Chem. Rev.* **2010**, *110* (5), 2641−2684.
(8) Qian, G.; Zhong, Z.; Luo, M.; Yu, D.; Zhang, Z.; Wang, Z. Y.; Ma, D. *Adv. Mater.* **2009**, *21* (1), 111−116.
(9) Borek, C.; Hanson, K.; Djurovich, P. I.; Thompson, M. E.; Aznavour, K.; Bau, R.; Sun, Y.; Forrest, S. R.; Brooks, J.; Michalski, L.; Brown, J. *Angew. Chem.* **2007**, *119* (7), 1127−1130.
(10) Ghoroghchian, P. P.; Frail, P. R.; Susumu, K.; Blessington, D.; Brannan, A. K.; Bates, F. S.; Chance, B.; Hammer, D. A.; Therien, M. J. *Proc. Natl. Acad. Sci. U. S. A.* **2005**, *102* (8), 2922−2927.
(11) Graham, K. R.; Yang, Y.; Sommer, J. R.; Shelton, A. H.; Schanze, K. S.; Xue, J.; Reynolds, J. R. *Chem. Mater.* **2011**, *23* (24), 5305−5312.
(12) Koide, Y.; Urano, Y.; Hanaoka, K.; Piao, W.; Kusakabe, M.; Saito, N.; Terai, T.; Okabe, T.; Nagano, T. *J. Am. Chem. Soc.* **2012**, *134* (11), 5029−5031.
(13) Yuan, L.; Lin, W.; Zhao, S.; Gao, W.; Chen, B.; He, L.; Zhu, S. *J. Am. Chem. Soc.* **2012**, *134* (32), 13510−13523.
(14) Yuan, L.; Lin, W.; Yang, Y.; Chen, H. *J. Am. Chem. Soc.* **2012**, *134* (2), 1200−1211.
(15) Bachmann, F. G.; Russek, U. A. In *Laser Welding of Polymers Using High-Power Diode Lasers*; SPIE: Bellingham, WA, 2002; pp 505−518.
(16) Fischer, G. M.; Daltrozzo, E.; Zumbusch, A. *Angew. Chem., Int. Ed.* **2011**, *50* (6), 1406−1409.
(17) Lunt, R. R.; Bulovic, V. *Appl. Phys. Lett.* **2011**, *98* (11), 113305.
(18) Xiao, L.; Su, Y.; Zhou, X.; Chen, H.; Tan, J.; Hu, T.; Yan, J.; Peng, P. *Appl. Phys. Lett.* **2012**, *101* (4), 041913.
(19) Wu, J. B.; Lin, T.-P.; Gallagher, J. D.; Kushal, S.; Chung, L. W. K.; Zhau, H. E.; Olenyuk, B. Z.; Shih, J. C. *J. Am. Chem. Soc.* **2015**, *137* (6), 2366−2374.
(20) Pansare, V. J.; Hejazi, S.; Faenza, W. J.; Prud'homme, R. K. *Chem. Mater.* **2012**, *24* (5), 812−827.
(21) Suzuki, H. *J. Photochem. Photobiol., A* **2004**, *166* (1−3), 155−161.
(22) Cai, K.; Xie, J.; Zhao, D. *J. Am. Chem. Soc.* **2014**, *136* (1), 28−31.
(23) Avlasevich, Y.; Mullen, K. *Chem. Commun.* **2006**, *42*, 4440−4442.
(24) Fischer, G. M.; Ehlers, A. P.; Zumbusch, A.; Daltrozzo, E. *Angew. Chem., Int. Ed.* **2007**, *46* (20), 3750−3753.
(25) Jiao, C.; Huang, K.-W.; Luo, J.; Zhang, K.; Chi, C.; Wu, J. *Org. Lett.* **2009**, *11* (20), 4508−4511.
(26) Karton-Lifshin, N.; Albertazzi, L.; Bendikov, M.; Baran, P. S.; Shabat, D. *J. Am. Chem. Soc.* **2012**, *134* (50), 20412−20420.
(27) Luo, M.; Shadnia, H.; Qian, G.; Du, X.; Yu, D.; Ma, D.; Wright, J. S.; Wang, Z. Y. *Chem. - Eur. J.* **2009**, *15* (35), 8902−8908.
(28) Mayerhöffer, U.; Fimmel, B.; Würthner, F. *Angew. Chem., Int. Ed.* **2012**, *51* (1), 164−167.
(29) Qian, G.; Dai, B.; Luo, M.; Yu, D.; Zhan, J.; Zhang, Z.; Ma, D.; Wang, Z. Y. *Chem. Mater.* **2008**, *20* (19), 6208−6216.
(30) Lu, X.; Fan, S.; Wu, J.; Jia, X.; Wang, Z.-S.; Zhou, G. *J. Org. Chem.* **2014**, *79* (14), 6480−6489.
(31) Umezawa, K.; Nakamura, Y.; Makino, H.; Citterio, D.; Suzuki, K. *J. Am. Chem. Soc.* **2008**, *130* (5), 1550−1551.
(32) Zhang, Z.; Edkins, R. M.; Nitsch, J.; Fucke, K.; Eichhorn, A.; Steffen, A.; Wang, Y.; Marder, T. B. *Chem. - Eur. J.* **2015**, *21* (1), 177−190.
(33) Parker, T. C.; Patel, D. G.; Moudgil, K.; Barlow, S.; Risko, C.; Bredas, J.-L.; Reynolds, J. R.; Marder, S. R. *Mater. Horiz.* **2015**, *2* (1), 22−36.
(34) Schwiderski, R. L.; Rasmussen, S. C. *J. Org. Chem.* **2013**, *78* (11), 5453−5462.
(35) Rasmussen, S. C.; Schwiderski, R. L.; Mulholland, M. E. *Chem. Commun.* **2011**, *47* (41), 11394−11410.
(36) Nietfeld, J. P.; Schwiderski, R. L.; Gonnella, T. P.; Rasmussen, S. C. *J. Org. Chem.* **2011**, *76* (15), 6383−6388.
(37) Schipper, D. J.; Fagnou, K. *Chem. Mater.* **2011**, *23* (6), 1594−1600.
(38) Liu, B.; Wang, Z.; Wu, N.; Li, M.; You, J.; Lan, J. *Chem. - Eur. J.* **2012**, *18* (6), 1599−1603.
(39) Zhang, J.; Chen, W.; Rojas, A. J.; Jucov, E. V.; Timofeeva, T. V.; Parker, T. C.; Barlow, S.; Marder, S. R. *J. Am. Chem. Soc.* **2013**, *135* (44), 16376−16379.
(40) Abdo, N. I.; El-Shehawy, A. A.; El-Barbary, A. A.; Lee, J.-S. *Eur. J. Org. Chem.* **2012**, *2012* (28), 5540−5551.
(41) Sugiura, H.; Nakai, Y.; Nomura, K. Organic thin film solar cell, monomers and organic semiconductor material composition used in organic thin film solar cell. Patent WO/2013/168709, 2013.
(42) Chao, C.-Y.; Chao, C.-H.; Chen, L.-P.; Hung, Y.-C.; Lin, S.-T.; Su, W.-F.; Lin, C.-F. *J. Mater. Chem.* **2012**, *22* (15), 7331−7341.
(43) Darabi, H. R.; Aghapoor, K.; Mohsenzadeh, F.; Jalali, M. R.; Talebian, S.; Ebadi-Nia, L.; Khatamifar, E.; Aghaee, A. *Bull. Korean Chem. Soc.* **2011**, *32* (1), 213−218.
(44) Park, C.-H.; Ryabova, V.; Seregin, I. V.; Sromek, A. W.; Gevorgyan, V. *Org. Lett.* **2004**, *6* (7), 1159−1162.
(45) Tang, S.-Y.; Guo, Q.-X.; Fu, Y. *Chem. - Eur. J.* **2011**, *17* (49), 13866−13876.
(46) Qin, C.; Clark, A. E. *Chem. Phys. Lett.* **2007**, *438* (1−3), 26−30.
(47) Rehm, D.; Weller, A. *Isr. J. Chem.* **1970**, *8* (2), 259−271.
(48) Zhang, Y.; Ren, P.; Li, Y.; Su, R.; Zhao, M. *J. Chem.* **2015**, *2015*, 402746.
(49) Lim, S.-Y.; Hong, K.-H.; Kim, D. I.; Kwon, H.; Kim, H.-J. *J. Am. Chem. Soc.* **2014**, *136* (19), 7018−7025.
(50) Ellinger, S.; Graham, K. R.; Shi, P.; Farley, R. T.; Steckler, T. T.; Brookins, R. N.; Taranekar, P.; Mei, J.; Padilha, L. A.; Ensley, T. R.; Hu, H.; Webster, S.; Hagan, D. J.; Van Stryland, E. W.; Schanze, K. S.; Reynolds, J. R. *Chem. Mater.* **2011**, *23* (17), 3805−3817.
(51) Meek, S. T.; Nesterov, E. E.; Swager, T. M. *Org. Lett.* **2008**, *10* (14), 2991−2993.
(52) Hassey, R.; Swain, E. J.; Hammer, N. I.; Venkataraman, D.; Barnes, M. D. *Science* **2006**, *314* (5804), 1437−1439.
(53) Xu, M.; Li, R.; Pootrakulchote, N.; Shi, D.; Guo, J.; Yi, Z.; Zakeeruddin, S. M.; Grätzel, M.; Wang, P. *J. Phys. Chem. C* **2008**, *112* (49), 19770−19776.
(54) Gawrys, P.; Marszalek, T.; Bartnik, E.; Kucinska, M.; Ulanski, J.; Zagorska, M. *Org. Lett.* **2011**, *13* (22), 6090−6093.
(55) Miao, Q.; Gao, J.; Wang, Z.; Yu, H.; Luo, Y.; Ma, T. *Inorg. Chim. Acta* **2011**, *376* (1), 619−627.

DOI: 10.1021/acs.joc.5b01958
J. Org. Chem. 2016, 81, 32−42

(56) Still, W. C.; Kahn, M.; Mitra, A. *J. Org. Chem.* **1978**, *43* (14), 2923−2925.
(57) Frisch, M. J.; Trucks, G. W.; Schlegel, H. B.; Scuseria, G. E.; Robb, M. A.; Cheeseman, J. R.; Scalmani, G.; Barone, V.; Mennucci, B.; Petersson, G. A.; Nakatsuji, H.; Caricato, M.; Li, X.; Hratchian, H. P.; Izmaylov, A. F.; Bloino, J.; Zheng, G.; Sonnenberg, J. L.; Hada, M.; Ehara, M.; Toyota, K.; Fukuda, R.; Hasegawa, J.; Ishida, M.; Nakajima, T.; Honda, Y.; Kitao, O.; Nakai, H.; Vreven, T.; Montgomery, J. A., Jr.; Peralta, J. E.; Ogliaro, F.; Bearpark, M. J.; Heyd, J.; Brothers, E. N.; Kudin, K. N.; Staroverov, V. N.; Kobayashi, R.; Normand, J.; Raghavachari, K.; Rendell, A. P.; Burant, J. C.; Iyengar, S. S.; Tomasi, J.; Cossi, M.; Rega, N.; Millam, N. J.; Klene, M.; Knox, J. E.; Cross, J. B.; Bakken, V.; Adamo, C.; Jaramillo, J.; Gomperts, R.; Stratmann, R. E.; Yazyev, O.; Austin, A. J.; Cammi, R.; Pomelli, C.; Ochterski, J. W.; Martin, R. L.; Morokuma, K.; Zakrzewski, V. G.; Voth, G. A.; Salvador, P.; Dannenberg, J. J.; Dapprich, S.; Daniels, A. D.; Farkas, Ö.; Foresman, J. B.; Ortiz, J. V.; Cioslowski, J.; Fox, D. J. *Gaussian 09*; Gaussian, Inc.: Wallingford, CT, 2009.
(58) Becke, A. D. *J. Chem. Phys.* **1993**, *98* (7), 5648−5652.
(59) Lee, C.; Yang, W.; Parr, R. G. *Phys. Rev. A: At., Mol., Opt. Phys.* **1988**, *37*, 785.
(60) Crosby, G. A.; Demas, J. N. *J. Phys. Chem.* **1971**, *75* (8), 991−1024.
(61) Magde, D.; Rojas, G. E.; Seybold, P. G. *Photochem. Photobiol.* **1999**, *70* (5), 737−744.
(62) Vincett, P. S.; Voigt, E. M.; Rieckhoff, K. E. *J. Chem. Phys.* **1971**, *55* (8), 4131−4140.

DOI: 10.1021/acs.joc.5b01958
J. Org. Chem. 2016, 81, 32−42